Hamburger Beiträge
zur Angewandten Mathematik

On an adaptive method for heat conduction problems with boundary layers

M. Breuß, V. Dolejší and A. Meister

Reihe F
Computational Fluid Dynamics and Data Analysis 14
May 2001

Hamburger Beiträge zur Angewandten Mathematik

Reihe A	Preprints
Reihe B	Berichte
Reihe C	Mathematische Modelle und Simulation
Reihe D	Elektrische Netzwerke und Bauelemente
Reihe E	Scientific Computing
Reihe F	Computational Fluid Dynamics and Data Analysis

On an adaptive method for heat conduction problems with boundary layers

M. Breuß*, V. Dolejší†and A. Meister*

June 5, 2001

Abstract

We deal with the numerical solution of heat conduction problems featuring steep gradients. In order to solve the associated partial differential equation a finite volume technique is used and unstructured grids are employed. A discrete maximum principle for triangulations of a Delaunay type is developed. To capture thin boundary layers incorporating steep gradients an anisotropic mesh adaptation technique is implemented. Computational tests are performed for an academic problem where the exact solution is known as well as for a real world problem of a computer simulation of the thermoregulation of premature infants.

Keywords: Finite volume method, Thermoregulation, Maximum principle, Anisotropic adaptation.

1 Introduction

The numerical simulation of flow phenomena often incorporates the evaluation of boundary layers or – more generally – of physical states which involve steep gradients of the occuring quantities, see [14, 15, 9]. This can be done

*Department of Mathematics, Center for Differential Equations und Dynamical Systems, University of Hamburg, Germany

†Department of Numerical Mathematics, Faculty of Mathematics and Physics, Charles University Prague, Czech Republic

either by the use of a sensible analytical approximation, e.g. by employing the Boussinesq approximation in a suitable situation [11], or by using a very fine grid near the boundary to achieve a valid numerical approximation of the flow field within the boundary layer. If a sensible numerical simulation of a flow phenomenon incorporating boundary layers can be done, this is by principle an advantage over an analytical approximation since the computed solution does not rely on additional physical assumptions concerning the situation at the boundary which have to be employed in an analytical approach. In other cases there is no analytical approximation available and the flow in the boundary layer has to be computed numerically anyway, e.g. in the case of nonlinear heat equations with source terms on a sophisticated domain featuring different boundary conditions. However, if the numerical simulation of the flow within a boundary layer is realized via an uniformly fine grid, the resulting computational problem easily becomes very large. Additionally, there is generally no way to predict how high the resolution actually has to be during the simulation depending on the initial values at the beginning of the computation. These considerations show that a flexible adaptive procedure is needed in the mentioned situation. Within this paper, we describe an adaptive procedure which is employed within a finite volume framework. The resulting method can be used to compute sophisticated flow fields with boundary layers in two spatial dimensions. In order to show the applicability of the method, several test cases are considered. This paper is organized accordingly. At first, we briefly describe the finite volume scheme recently introduced by Fischer et al. [8]. In the following, a discrete formulation of the minimum-maximum principle is proven for special situations, whereby compared to [8] weaker assumptions concerning the underlying primary mesh are used. After that, the used anisotropic mesh adaptation technique is introduced. Then it follows a section where applications of two types are considered. We compare several analytical solutions featuring strong boundary layers with results computed with the help of the described method. Afterwards the method is applied to a real world problem, namely a model of thermoregulation of premature infants.
The mathematical problems under consideration are given by variations of the heat equation

$$\partial_t T(\mathbf{x}, t) = \operatorname{div}\left(\lambda(\mathbf{x}) \nabla T(\mathbf{x}, t)\right) + q(\mathbf{x}, t), \tag{1}$$

where $\mathbf{x} = (x_1, x_2)^T \in \Omega \subset \mathbb{R}^2$ and $t \in \mathbb{R}^+$. Additionally, initial and boundary conditions of various types are employed. As indicated before, the spatial domain Ω may be non-convex and quite sophisticated depending on the concrete application.

2 Numerical Method

Finite volume methods have proven to be reliable and accurate approximation techniques for a great variety of conservation laws with and without source terms [14, 15, 16, 12, 8, 6, 7]. These schemes are formulated on general control volumes and well-known successful time stepping schemes and spatial discretization techniques can easily be employed in the general framework. We call a bounded subset $\sigma \subset \mathbb{R}^2$ a control volume or box if its boundary is at least Lipschitz continuous. This requirement enables the application of the Gauss integral theorem. Introducing the cell average operator

$$\left.(\mathcal{M}T)(t)\right|_\sigma := \frac{1}{|\sigma|}\int_\sigma T(\mathbf{x},t)\,d\mathbf{x}, \tag{2}$$

the function T is called a weak solution of equation (1), if

$$\frac{d}{dt}\left.(\mathcal{M}T)(t)\right|_\sigma = -\frac{1}{|\sigma|}\int_{\partial\sigma}\lambda(\mathbf{x})\nabla T(\mathbf{x},t)\cdot\mathbf{n}\,ds + \frac{1}{|\sigma|}\int_\sigma q(\mathbf{x},t)\,d\mathbf{x} \tag{3}$$

holds for all control volumes $\sigma \subset \Omega$, where $|\sigma|$ and $\mathbf{n}$ denote the area of the box σ and the unit outer normal vector on $\partial\sigma$, respectively. For simplicity, we assume the boundary $\partial\Omega$ to be smooth in the sense that it can be approximated by a finite number of straight lines in a sufficiently accurate manner (for example, $\partial\Omega$ is piecewise polygonal). In order to obtain an appropriate decomposition of the domain Ω into a finite number of control volumes, we start from an arbitrary conforming triangulation $\mathcal{D}_h$ of the domain Ω which is called the primary mesh consisting of finitely many (say $\#\mathcal{D}_h$) triangles $\mathcal{D}_i$, $i \in I = \{1,\ldots,\#\mathcal{D}_h\}$. For a comprehensive definition of a primary grid we refer to Sonar [17]. Furthermore, $\mathcal{N}_h$ denotes the index set of all nodes of the triangulation $\mathcal{D}_h$ and is subdivided by $\mathcal{N}_h = \mathcal{N}_h^{\mathcal{D}_h} \cup \mathcal{N}_h^{\partial\mathcal{D}_h}$, where $\mathcal{N}_h^{\mathcal{D}_h}$ is associated with the inner points and $\mathcal{N}_h^{\partial\mathcal{D}_h}$ includes the indices of the boundary points. We set $N := \#\mathcal{N}_h$ and denote the three edges of the triangle $\mathcal{D}$ by $e_{\mathcal{D},k}$, $k = 1,2,3$. Furthermore, we define

$$E(i) = \left\{e_{\mathcal{D},k}\,|\; k \in \{1,2,3\}, \mathcal{D} \in \mathcal{D}_h,\ \text{node}\ \mathbf{x}_i \in e_{\mathcal{D},k}\right\},$$

$$V(i) = \{\mathcal{D} |\text{ node } \mathbf{x}_i \text{ is vertex of } \mathcal{D} \in \mathcal{D}_h\},$$

and

$$C(\mathcal{D}) = \{i | i \in \{1, \ldots, N\}, \text{ node } \mathbf{x}_i \text{ is vertex of } \mathcal{D}\}.$$

Concerning the weak formulation (3) of the governing equation (1), the occurrence of second order derivatives within the partial differential equation (1) requires the evaluation of first order derivatives on the boundary of each control volume used within the finite volume scheme. Due to this fact we decided to employ a box type method where the computation of a first order derivative on the boundary of each box is straightforward. For the numerical approximation of the involved integrals we follow the proceeding described in [8] which we now briefly explain. We define a discrete control volume σ_i as the open subset of $\mathbb{R}^2$ including the node $\mathbf{x}_i = (x_{i1}, x_{i2})^T$ and bounded by the straight lines defined by the connection of the midpoint of the edge $e_{\mathcal{D},k} \in E(i)$ with the barycentre $\mathbf{x}_s = (x_{s1}, x_{s2})^T = \frac{1}{3}\sum_{i \in C(\mathcal{D})} \mathbf{x}_i$ of the corresponding triangle $\mathcal{D}$ (see Figure 1). In the case that $\mathbf{x}_i$ is on the boundary of the computational domain, the line defined by the connection of the midpoint of the boundary edge and the node itself is also a part of $\partial\sigma_i$. The union $\mathcal{B}_h$ of all boxes σ_i, $i \in \mathcal{N}_h$, is called the secondary mesh. Let $N(i)$ denote the index set of all nodes neighboring node $\mathbf{x}_i$, i.e. those nodes $\mathbf{x}_j$, $j \neq i$, for which $\int_{\partial\sigma_i \cap \partial\sigma_j} 1 \, ds \neq 0$ is valid. In general, for $j \in N(i)$ the boundary between the control volume σ_i and σ_j consists of two line segments which are denoted by l_{ij}^k, $k = 1, 2$. Furthermore, $\mathbf{n}_{ij}^k$, $k = 1, 2$, represent the accompanying unit normal vectors (see Figure 1 (right)).

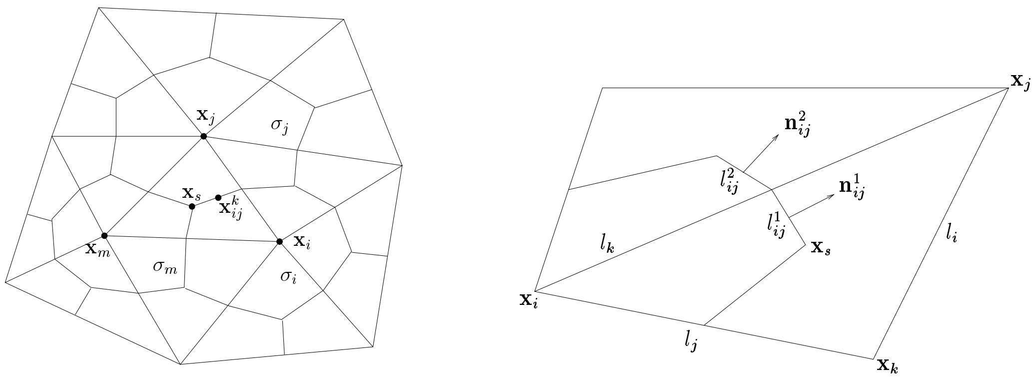

Figure 1: Triangulation and boxes (left). Geometry between boxes (right).

With regard to the secondary mesh $\mathcal{B}_h$ we can rewrite the integral form of the heat equation as

$$
\begin{aligned}
\frac{d}{dt}\underbrace{\left(\mathcal{M}T\right)(t)|_{\sigma_i}}_{=:\,T_i(t)} &= -\frac{1}{|\sigma_i|}\sum_{j\in N(i)}\sum_{k=1}^{2}\int_{l_{ij}^k}\lambda(\mathbf{x})\nabla T(\mathbf{x},t)\cdot\mathbf{n}(\mathbf{x})\,ds \\
&\quad +\frac{1}{|\sigma_i|}\int_{\sigma_i} q(\mathbf{x},t)\,d\mathbf{x},\ \ \forall\sigma_i\in\mathcal{B}_h.
\end{aligned}
$$

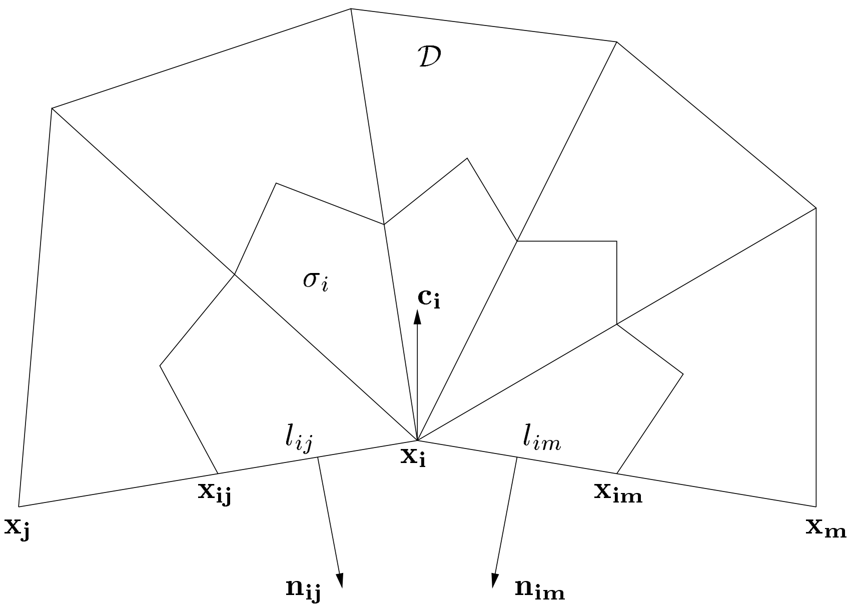

Figure 2: Boundary control volume

Taking account of the secondary mesh $\mathcal{B}_h$ and using a unique linear distribution of T as well as the mean value of the heat conductivity $\lambda_{\mathcal{D}}$ on each triangle $\mathcal{D}$ of the primary grid directly leads to the formulation of a numerical flux function

$$
H\left(T_i(t),T_j(t),T_m(t);\mathbf{n}_{ij}^k\right) = \lambda_{\mathcal{D}}\nabla T_{\mathcal{D}}(t)\cdot\mathbf{n}_{ij}^k.
$$

Consequently, for each inner control volume we obtain

$$\int_{\partial\sigma_i} \lambda(\mathbf{x})\nabla T(\mathbf{x},t)\cdot\mathbf{n}(\mathbf{x})\; ds = \sum_{j\in N(i)}\sum_{k=1}^{2} H\left(T_i(t), T_j(t), T_m(t); \mathbf{n}_{ij}^k\right)|l_{ij}^k|.$$

A convenient numerical approximation of the remaining boundary integral is required in order to ensure a discrete minimum maximum principle in our numerical framework. Utilizing the notation introduced within Figure 2, Fischer et al. [8] proposed the definition of an extended barycenter

$$\mathbf{c}_i = \mathbf{x}_i - \frac{\sqrt{3}\rho_i}{4\|\mathbf{n}_{ij}+\mathbf{n}_{im}\|_2}(\mathbf{n}_{ij}+\mathbf{n}_{im}), \tag{4}$$

with a certain weight

$$\rho_i = \frac{1}{2}\min\{\|\mathbf{x}_j - \mathbf{x}_i\|_2 \,|\, j\in N(i)\cap C(\mathcal{D})\}.$$

Hence the remaining boundary integral is approximated as

$$\int\limits_{\partial\sigma_i\cap\partial\Omega} \lambda(\mathbf{x})\nabla T(\mathbf{x},t)\cdot\mathbf{n}(\mathbf{x})\; ds = \sum_{\ell\in\{j,m\}} H(T_i(t), T_{i,\partial\Omega}(\mathbf{x}_i), T_{i,\partial\Omega}(\mathbf{x}_{i\ell}); \mathbf{n}_{i\ell})\,|l_{i\ell}|\,,$$

where the physical quantities T_i, $T_{i,\partial\Omega}(\mathbf{x}_i)$ and $T_{i,\partial\Omega}(\mathbf{x}_{i\ell})$ are assumed to be located at the nodes $\mathbf{c}_i$, $\mathbf{x}_i$ and $\mathbf{x}_{i\ell}$, respectively, and the gradient ∇T is computed using the triangle built by the above mentioned nodes. A simple approximation of the source term yields

$$\frac{1}{|\sigma_i|}\int_{\sigma_i} q(\mathbf{x},t)\; d\mathbf{x} = q(\mathbf{x}_i,t).$$

For the approximation of the temporal derivative a forward or backward Euler time step technique is employed, whereby the source term is always evaluated in an explicit manner. Thus, the whole numerical method can be written as

$$\begin{aligned} T_i^{n+1} &= T_i^n - \frac{\Delta t}{|\sigma_i|}\Big\{\sum_{j\in N(i)}\sum_{k=1}^{2} H\left(T_i^m, T_j^m, T_m^m; \mathbf{n}_{ij}^k\right)|l_{ij}^k| \\ &\qquad +\delta_i \sum_{\ell\in\{j,m\}} H(T_i^m, T_{i,\partial\Omega}(\mathbf{x}_i), T_{i,\partial\Omega}(\mathbf{x}_{i\ell}); \mathbf{n}_{i\ell})\,|l_{i\ell}|\Big\} + \Delta t q_i^n, \end{aligned} \tag{5}$$

where $m \in \{n, n+1\}$, $\Delta t = t^{n+1} - t^n$, $T_i^n = T_i(t^n)$, $q_i^n = q(\mathbf{x}_i, t^n)$ and

$$\delta_i = \begin{cases} 1, & \text{if } i \in \mathcal{N}_h^{\partial \mathcal{D}_h} \\ 0, & \text{otherwise.} \end{cases}$$

Fischer et al. [8] proved that the described finite volume scheme satisfies a discrete minimum maximum principle in the absence of source terms if the underlying primary mesh consists exclusively of triangles $\mathcal{D}_i$ whose inner angles are less or equal 90°.
The consideration of finitely many different tissues within the modelling process of realistic heat conduction problems often yields a heat equation where the heat conductivity is constant almost everywhere. In such a case we usually obtain that the majority of the boxes $\sigma_i \in \mathcal{B}_h$ satisfies the property $\lambda_{\mathcal{D}} = \lambda_{\widetilde{\mathcal{D}}}$ for all accompanying triangles $\mathcal{D}, \widetilde{\mathcal{D}} \in V(i)$. Examples are given by the following academic test case (19) as well as by the realistic model (21) which is actually employed for the thermoregulation of premarure infants within industrial applications.[1]. In this context we are able to improve the minimum maximum principle developed in [8] in the sense that weaker conditions on the underlying primary mesh $\mathcal{D}_h$ have to be required. More precisely, angles greater than 90° are allowed within the triangulation $\mathcal{D}_h$. In the following we assume that the primary grid $\mathcal{D}_h$ satisfies the properties

- A1: The triangulation $\mathcal{D}_h$ is of Delaunay type, whereby the sum of opposite angles α_j, α_ℓ is less than π for any pair of neighbouring triangles, see Figure 3,

- A2: The opposite angle α with respect to a boundary edge is less than $\pi/2$, see Figure 4 (right).

First, we consider an inner control volume.

Lemma 2.1 *Let $\mathcal{D}_h$ and T_i^n, $i \in \mathcal{N}_h^{\mathcal{D}_h}$, satisfy the condition* A1 *and*

$$T_i^n \geq \max_{j \in N(i)} T_j^n.$$

Then the update fulfills

$$\sum_{j \in N(i)} \sum_{k=1}^{2} H(T_i^n, T_j^n, T_m^n; \mathbf{n}_{ij}^k)|l_{ij}^k| = 0 \tag{6}$$

if and only if

$$T_i^n = T_j^n$$

holds for all $j \in N(i)$.

Proof:

Since both the heat conductivity $\lambda_{\mathcal{D}}$ as well as the gradient of the temperature distribution $\nabla T_{\mathcal{D}}$ are constant on each triangle $\mathcal{D} \in \mathcal{D}_h$ we obtain by means of the notation depicted in Figures 4 (left) and 3

$$\sum_{\ell \in \{j,m\}} H(T_i^n, T_j^n, T_m^n; \mathbf{n}_{i\ell})|l_{i\ell}| = \frac{1}{2} H(T_i^n, T_j^n, T_m^n; \mathbf{n}_{\mathcal{D}_j}^i)$$

where $\mathbf{n}_{\mathcal{D}_j}^{\xi}$ represents the outer normal vector on $\mathbf{e}_{\mathcal{D}_j}^{\xi}$, $\xi \in \{i, j, m\}$, with $\left|\mathbf{n}_{\mathcal{D}_j}^{\xi}\right| = \left|\mathbf{e}_{\mathcal{D}_j}^{\xi}\right|$. Thus, we get

$$\sum_{j \in N(i)} \sum_{k=1}^{2} H(T_i^n, T_j^n, T_m^n; \mathbf{n}_{ij}^k)|l_{ij}^k| = \frac{1}{2} \sum_{j \in N(i)} H(T_i^n, T_j^n, T_m^n; \mathbf{n}_{\mathcal{D}_j}^i). \tag{7}$$

Let ϕ_j^{ξ}, $\xi \in \{i, j, m\}$, denote the three linear functions on $\mathcal{D}_j$ satisfying

$$\phi_j^{\xi}(\mathbf{x}_k) = \begin{cases} 1 & , \xi = k \in \{i, j, m\} \\ 0 & , \text{otherwise} \end{cases}$$

then the gradient of the temperature with respect to the triangle $\mathcal{D}_j$ writes

$$\nabla T_{\mathcal{D}_j} = T_i \nabla \phi_j^i + T_j \nabla \phi_j^j + T_m \nabla \phi_j^m$$

with

$$\nabla \phi_j^{\xi} = -\frac{\mathbf{n}_{\mathcal{D}_j}^{\xi}}{2|\mathcal{D}_j|}, \ \xi \in \{i, j, m\}.$$

Consequently, the numerical flux function can be expressed as

$$H(T_i^n, T_j^n, T_m^n; \mathbf{n}_{\mathcal{D}_j}^i) = -\frac{\lambda_{\mathcal{D}_j}}{2|\mathcal{D}_j|} \left(T_i^n \mathbf{n}_{\mathcal{D}_j}^i + T_j^n \mathbf{n}_{\mathcal{D}_j}^j + T_m^n \mathbf{n}_{\mathcal{D}_j}^m \right) \mathbf{n}_{\mathcal{D}_j}^i.$$

Using $\lambda_{\mathcal{D}_m} = \lambda_{\mathcal{D}_\ell} =: \lambda$ for all $\mathcal{D}_m, \mathcal{D}_\ell \in V(i)$ together with equation (7) yields

$$
\begin{aligned}
&\sum_{j\in N(i)} \sum_{k=1}^{2} H(T_i^n, T_j^n, T_m^n; \mathbf{n}_{ij}^k)|l_{ij}^k| \\
&\quad = -\frac{\lambda}{4} \sum_{j\in N(i)} \frac{1}{|\mathcal{D}_j|} \left(T_i^n \mathbf{n}_{\mathcal{D}_j}^i + T_j^n \mathbf{n}_{\mathcal{D}_j}^j + T_m^n \mathbf{n}_{\mathcal{D}_j}^m \right) \mathbf{n}_{\mathcal{D}_j}^i \\
&\quad = -\frac{\lambda}{4} T_i^n \sum_{j\in N(i)} \underbrace{\left(\mathbf{n}_{\mathcal{D}_j}^i + \mathbf{n}_{\mathcal{D}_j}^j + \mathbf{n}_{\mathcal{D}_j}^m \right)}_{=0} \frac{\mathbf{n}_{\mathcal{D}_j}^i}{|\mathcal{D}_j|} \\
&\qquad + \frac{\lambda}{4} \sum_{j\in N(i)} \epsilon_j^n \left(\frac{\mathbf{n}_{\mathcal{D}_j}^i \mathbf{n}_{\mathcal{D}_j}^j}{|\mathcal{D}_j|} + \frac{\mathbf{n}_{\mathcal{D}_\ell}^i \mathbf{n}_{\mathcal{D}_\ell}^j}{|\mathcal{D}_\ell|} \right), \qquad (8)
\end{aligned}
$$

where $\epsilon_j^n := T_i^n - T_j^n \geq 0$. Using for $k \in \{\ell, j\}$

$$
\mathbf{n}_{\mathcal{D}_k}^i \mathbf{n}_{\mathcal{D}_k}^j = -\left|\mathbf{n}_{\mathcal{D}_k}^i\right| \left|\mathbf{n}_{\mathcal{D}_k}^j\right| \cos \alpha_k
$$

and

$$
|\mathcal{D}_k| = \frac{1}{2} \left|\mathbf{n}_{\mathcal{D}_k}^i\right| \left|\mathbf{n}_{\mathcal{D}_k}^j\right| \sin \alpha_k
$$

one obtains

$$
\begin{aligned}
\frac{\mathbf{n}_{\mathcal{D}_j}^i \mathbf{n}_{\mathcal{D}_j}^j}{|\mathcal{D}_j|} + \frac{\mathbf{n}_{\mathcal{D}_\ell}^i \mathbf{n}_{\mathcal{D}_\ell}^j}{|\mathcal{D}_\ell|} &= -\frac{2\cos \alpha_j}{\sin \alpha_j} - \frac{2\cos \alpha_\ell}{\sin \alpha_\ell} \\
&= -2 \frac{\cos \alpha_j \sin \alpha_\ell + \cos \alpha_\ell \sin \alpha_j}{\sin \alpha_j \sin \alpha_\ell} \\
&= -2 \frac{\sin(\alpha_j + \alpha_\ell)}{\sin \alpha_j \sin \alpha_\ell} \overset{\mathsf{A1}}{<} 0. \qquad (9)
\end{aligned}
$$

Inserting equation (9) into (8) leads to the statement that (6) is equivalent to $\epsilon_j^n = 0$ for all $j \in N(i)$ which completes the proof. □

To obtain a physical senseful approximation of the fluxes at the boundary of the computational domain $\partial\Omega$ it is not necessary to require any additional assumptions concerning the primary mesh $\mathcal{D}_h$. The property of the numerical fluxes are completely determined by the definition (4) of the extended barycenter $\mathbf{c}_i$. Thus, we can take over the following statement which is proven in [8].

Lemma 2.2 *Let $i \in \mathcal{N}_h^{\partial \mathcal{D}_h}$ and $j \in N(i) \cap \mathcal{N}_h^{\partial \mathcal{D}_h}$, then the local update associated with the edge l_{ij}*

$$\Delta T_i|_{l_{ij}} = -\frac{\Delta t}{|\sigma_i|} H(T_i^n, T_{i,\partial\Omega}(\mathbf{x}_i), T_{i,\partial\Omega}(\mathbf{x}_{i\ell}); \mathbf{n}_{i\ell})\, |l_{i\ell}|$$

satiesfies

$$\Delta T_i|_{l_{ij}} \leq 0 \;\; (\Delta T_i|_{l_{ij}} < 0)$$

if

$$T_i^n \geq T_{i,\partial\Omega} \;\; (T_i^n > T_{i,\partial\Omega})$$

holds.

Since Lemma 2.2 can be easily formulated in the same manner replacing the inequality signs $\geq$, $>$ by $\leq$, $<$ and vice versa, we get the following statement

Lemma 2.3 *Let $i \in \mathcal{N}_h^{\partial \mathcal{D}_h}$ and $j \in N(i) \cap \mathcal{N}_h^{\partial \mathcal{D}_h}$, then the local update associated with the edge l_{ij}*

$$\Delta T_i|_{l_{ij}} = -\frac{\Delta t}{|\sigma_i|} H(T_i^n, T_{i,\partial\Omega}(\mathbf{x}_i), T_{i,\partial\Omega}(\mathbf{x}_{i\ell}); \mathbf{n}_{i\ell})\, |l_{i\ell}|$$

satiesfies

$$\Delta T_i|_{l_{ij}} = 0$$

if and only if

$$T_i^n = T_{i,\partial\Omega}$$

holds.

A close inspection of the proof of Lemma 2.1 shows that one can easily carry over the statement concerning the inner boxes to the boundary control volumes by means of Lemma 2.2. Consequently we obtain the novel version of the minimum maximum principle.

Theorem 2.4 *Given a steady state solution $T_i^{n+1} = T_i^n$ and a vanishing source term q_i^n for all $i \in \{1, \ldots, N\}$. If there exists an index $i \in \mathcal{N}_h$ such that*

$$T_i^n = \max_{\ell \in \mathcal{N}_h, j \in \mathcal{N}_h^{\partial \mathcal{D}_h}} \{T_\ell^n, T_{j,\partial\Omega}\}$$

than

$$T_\ell^n = T_i^n = T_{j,\partial\Omega}$$

holds for all $\ell \in \mathcal{N}_h$ and $j \in \mathcal{N}_h^{\partial \mathcal{D}_h}$.

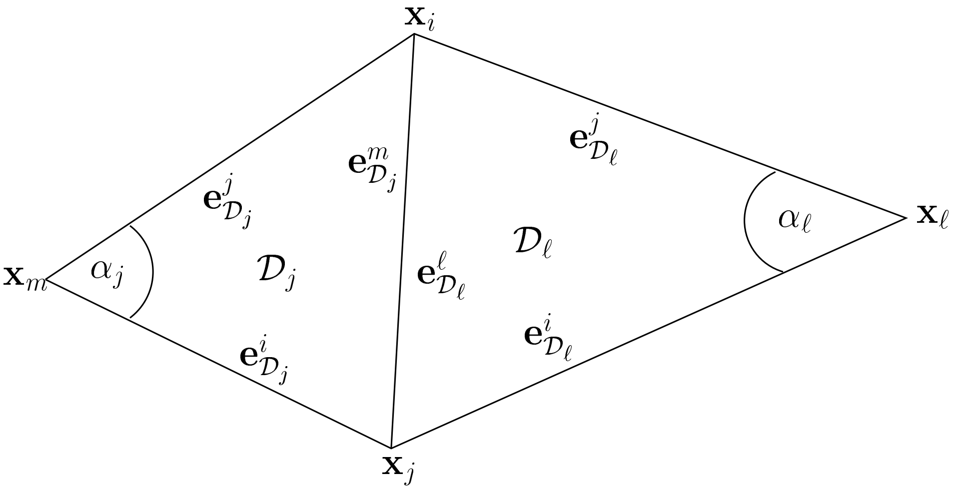

Figure 3: Notation within adjacent triangles concerning σ_i and σ_j

Proof:

If $i \in \mathcal{N}_h^{\mathcal{D}_h}$ than it follows directly from Lemma 2.1 that there exists at least one $j \in \mathcal{N}_h^{\partial\mathcal{D}_h}$ such that $T_i^n = T_j^n$. Thus, without loss of generality we can focus our attention to the case $i \in \mathcal{N}_h^{\partial\mathcal{D}_h}$. Decomposing the computation of the update $T_i^{n+1} - T_i^n$ into three terms and using an argumentation similar to the proof of Lemma 2.1 we can write

$$T_i^{n+1} - T_i^n = \frac{\Delta t}{|\sigma_i|}\left(U_1 + U_2 + U_3\right)$$

with

$$U_1 = -\underbrace{\frac{\lambda}{2}}_{>0} \sum_{j \in N(i) \cap \mathcal{N}_h^{\mathcal{D}_h}} \underbrace{\left(T_i^n - T_j^n\right)}_{=\epsilon_j^n \geq 0} \underbrace{\frac{\sin(\alpha_\ell + \alpha_j)}{\sin\alpha_\ell \sin\alpha_j}}_{\overset{\text{A1}}{>0}} \leq 0,$$

$$U_2 = -\underbrace{\frac{\lambda}{2}}_{>0} \sum_{j \in N(i) \cap \mathcal{N}_h^{\partial\mathcal{D}_h}} \underbrace{\left(T_i^n - T_j^n\right)}_{=\epsilon_j^n \geq 0} \underbrace{\frac{\cos\alpha_j}{\sin\alpha_j}}_{\overset{\text{A2}}{>0}} \leq 0,$$

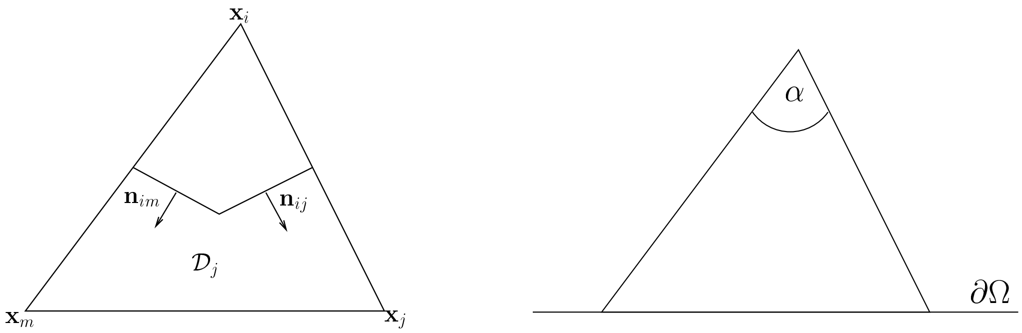

Figure 4: Notation within triangle $\mathcal{D}_j$ (left), boundary triangle (right)

$$U_3 \;=\; -\sum_{\ell\in\{j,m\}} H(T_i^n, T_{i,\partial\Omega}(\mathbf{x}_i), T_{i,\partial\Omega}(\mathbf{x}_{i\ell}); \mathbf{n}_{i\ell})\,|l_{i\ell}| \overset{\text{Lemma2.2}}{\leq} 0.$$

Thus, we obtain $U_1 = U_2 = U_3 = 0$. The property $U_1 = U_2 = 0$ directly proves $\epsilon_j^n = T_i^n - T_j^n = 0$ for all $j \in N(i)$. Furthermore $U_3 = 0$ yields $T_i^n = T_{i,\partial\Omega}(\mathbf{x}_i) = T_{i,\partial\Omega}(\mathbf{x}_{ij})$ for all $j \in N(i) \cap \mathcal{N}_h^{\partial\mathcal{D}_h}$ using Lemma 2.3. A successive repetition of this argumentation finally yields the statement. $\square$

3 Anisotropic adaptation

In order to obtain sufficiently accurate numerical approximations of the real solution we refine the grid in regions with steep gradients. Therefore we apply the anisotropic mesh adaptation (AMA) method which is suitable to adapt a given triangulation with the aim that the new number of elements is as small as possible. A sophisticated description of the AMA method is given in [4] while a thorough description of its theoretical background together with some further improvements can be found in [5]. We here only give a brief presentation of the AMA technique.

3.1 Theoretical background

Let $\mathcal{D}_h = \{\mathcal{D}_i\}_{i\in I}$ ($I =$ an index set) be a triangulation of the computational domain Ω. Let T be the exact solution of the continuous problem (1) and T_h

the approximate solution given by the numerical scheme (5). We recall that the numerical solution T_h depends on $\mathcal{D}_h$. Now, we proceed with

Definition 3.1 *Let T and T_h be the exact and numerical solution of the problem (1), respectively. The interpolation error function $\eta_I(\mathbf{x})$ is given by (see [5, 3])*

$$\eta_I(\mathbf{x}) = |T(\mathbf{x}) - T_h(\mathbf{x})|, \ \mathbf{x} \in \Omega. \tag{10}$$

Let $\omega > 0$ be a given tolerance. Our aim is to adapt the triangulation $\mathcal{D}_h$ in a way that the interpolation error function satisfies the condition

$$\eta_I(\mathbf{x}) \leq \omega, \qquad \text{for all } \mathbf{x} \in \Omega. \tag{11}$$

In [5] a necessary condition on $\mathcal{D}_h$ is derived so that the relation (11) is fulfilled. That necessary condition depends on the exact solution T and not on the approximate solution T_h. The task is now to define a triangulation satisfying the necessary condition described in [5] while the number of elements is as small as possible. Therefore, let $\mathcal{E}_h = \{e_k\}_{k \in K}$ (K= an index set) be the set of all edges of the triangulation $\mathcal{D}_h$. By $Q_k, \ k \in K$, we denote the center of e_k. Let us suppose that the exact solution T has continuous second order derivatives with respect to the spatial variables, i.e. $T \in C^2(\Omega)$. Additionally, we assume that a sensible continuation of the second order derivatives to the boundary of Ω can be defined, i.e. we write $T \in C^2(\overline{\Omega})$. We define $\boldsymbol{H}_k, \ k \in K$, as the Hessian matrix evaluated in Q_k

$$\boldsymbol{H}_k = \left. \begin{pmatrix} \dfrac{\partial^2 T}{\partial x_1^2} & \dfrac{\partial^2 T}{\partial x_1 \partial x_2} \\ \dfrac{\partial^2 T}{\partial x_1 \partial x_2} & \dfrac{\partial^2 T}{\partial x_2^2} \end{pmatrix} \right|_{Q_k}, \qquad k \in K. \tag{12}$$

Moreover we suppose that $\boldsymbol{H}_k, \ k \in K$, are positive definite matrices. We define the norm of the edge e_k corresponding to $\boldsymbol{H}_k$ by

$$\|e_k\|_{\boldsymbol{H}_k} := \left(e_k^{\mathrm{T}} \boldsymbol{H}_k e_k\right)^{\frac{1}{2}}, \tag{13}$$

where e_k is considered as a column vector in $\mathbb{R}^2$, e_k^{T} is the transposed vector and $e_k^{\mathrm{T}} \boldsymbol{H}_k e_k$ denotes the corresponding vector-matrix-vector product.
Now we proceed to the following

Definition 3.2 *Let $\mathcal{D}_h$ be a triangulation of the computational domain Ω and $\mathcal{E}_h = \{e_k\}_{k\in K}$ be the set of all edges of $\mathcal{D}_h$. Let $T \in C^2(\overline{\Omega})$ be the exact solution of (1) and the Hessian matrices $\boldsymbol{H}_k,\ k \in K$, given by (12) are positively definite. We say that the triangulation $\mathcal{D}_h$ is* edge-optimal*, if*

$$\|e_k\|_{\boldsymbol{H}_k} = \sqrt{6\omega} \qquad \forall k \in K. \tag{14}$$

We now define a parameter which indicates how close the triangulation $\mathcal{D}_h$ is to the edge-optimal one.

Definition 3.3 *Let $\mathcal{D}_h$ be a triangulation of Ω and let $\mathbf{H}_k$ be a symmetric positive definite 2×2 matrix defined for each node $e_k,\ k \in K$, of $\mathcal{D}_h$. Then the quality parameter of the triangulation $\mathcal{D}_h$ is given by*

$$Q_{\mathcal{D}_h} = \frac{1}{\#\mathcal{E}_h} \sum_{k\in K} \left(\|e_k\|_{\boldsymbol{H}_k} - \sqrt{6\omega}\right)^2, \tag{15}$$

where $\|e_k\|_{\boldsymbol{H}_k}$ is the norm of the edge e_k of $\mathcal{D}_h$ and $\#\mathcal{E}_h$ denotes the number of edges of $\mathcal{D}_h$.

It is clear that $Q_{\mathcal{D}_h} \geq 0$ is always satisfied and it is also clear that $Q_{\mathcal{D}_h} = 0$ holds if the mesh $\mathcal{D}_h$ is edge-optimal. The aim is now to adapt a given triangulation in order to minimize the quality parameter $Q_{\mathcal{D}_h}$.

3.2 Optimization of the mesh

Of course it is practically not possible to set the matrixes $\boldsymbol{H}_k,\ k \in K$, according to (12) because we do not know the exact solution T. Instead of T we use a smoothed version of the approximate numerical solution T_h which we denote as $\tilde{T}_h$, for more detail see [4] or [5]. In general, the matrices $\boldsymbol{H}_k,\ k \in K$, are symmetric but not positive definite. Moreover, they can be singular (e.g. if $\tilde{T}_h$ is linear on Ω). To overcome these difficulties, we define matrices

$$\boldsymbol{M}_k = c\left[\mathbf{I} + \alpha(\|\boldsymbol{H}_k\|)|\boldsymbol{H}_k|\right], \quad k \in K, \tag{16}$$

where $c > 0$ is a constant and $\alpha(\|\boldsymbol{H}_k\|)$ is a function of the norms of the matrix $\boldsymbol{H}_k$. We put $\|\boldsymbol{H}\| = \max_{i,j=1,2} |h_{ij}|$, where $h_{ij},\ i,j = 1,2$, are the elements of $\boldsymbol{H}$. The symbol $|\boldsymbol{H}_k|$ denotes the absolute value of the matrix $\boldsymbol{H}_k$ described as follows. As $\boldsymbol{H}_k$ is symmetric, it can be diagonalized by

$$\boldsymbol{H}_k = \mathbf{R}_k \mathrm{diag}(\lambda_{k1}, \lambda_{k2}) \mathbf{R}_k^{-1},\ k \in K, \tag{17}$$

where $\lambda_{k1}, \lambda_{k2}$ are the eigenvalues of $\boldsymbol{H}_k$ and $\mathbf{R}_k$ is the matrix composed of the columns of eigenvectors of $\boldsymbol{H}_k$. We put

$$|\boldsymbol{H}_k| = \mathbf{R}_k \mathrm{diag}(|\lambda_{k1}|, |\lambda_{k2}|)\mathbf{R}_k^{-1},\ k \in K. \tag{18}$$

Now we define an iterative process which consists of a finite combination of the following local operations on the mesh:

- Adding a node in the center of an edge,
- Removing an edge,
- Swapping the diagonal of the quadrilateral formed by any pair of adjacent elements,
- Moving a node into a more suitable position.

These operations are performed in order to decrease the quality parameter $Q_{\mathcal{D}_h}$, for more details see [4, 5].

4 Applications

The mathematical modelling of heat conduction phenomena leeds to variations of the governing model equation (1). In a concrete situation this equation can incorporate considerable source terms which can result in strong heat gradients at the boundary of the domain of interest while the heat distribution in the core of the domain features comparatively less variation. In order to compute a valid numerical approximation, such types of solutions pose the difficulty that a much more higher resolution is needed near the boundary of the domain than in its core. In the following, we consider two types of applications of the described method to heat flow problems. First, we have a look at a simple model situation where the computation of an analytic solution is possible. This model problem features a parameter θ which gives solutions with boundary layers of different strengths depending on its value, and we compare some exact solutions with the corresponding results from the described numerical method. At second, we consider a model of thermoregulation of premature infants. For more information concerning that topic, see [1, 18, 19]. In this case, our interest is not focused on the comparison with an exact solution which is not available, but we investigate the number of triangles needed in order to discretize the employed two-dimensional form of the shape of an infant. We then compare the number of triangles that the adaptive scheme needs with the number of triangles used within a corresponding model investigated by Fischer et al. [8] which does not feature an adaptive routine.

4.1 Boundary layer problem with analytic solution

The governing equation of the problem under consideration is given by

$$\partial_t T(\mathbf{x}, t) = \mathrm{div} \nabla T(\mathbf{x}, t) + y''(x_1) \tag{19}$$

where we set $y(x_1) = x_1^\theta$ with $\theta \bmod 2 = 0$. The domain of interest is given by $[-1, 1] \times [-1, 1] \subset \mathbb{R}^2$ where we employ periodic boundary conditions at the boundaries parallel to the x_1-axis and the Dirichlet condition $T = 1$ at the boundaries parallel to the x_2-axis. Additionally, a fixed line is set along the x_1-axis where we will later measure the values of the quantity T within the control volumes are measured in order to compare these data with the values of the exact solution. As can easily be verified, the analytical steady state solution of the described problem depends only on x_1 and is given by

$$T(x_1) = 2 - x_1^\theta. \tag{20}$$

At first, we set $\theta = 6$. We start the steady state computations with a very coarse grid, see Figure 5 on page 22. To the right of that grid a comparison of the values of different numerical solutions along the x_1-axis corresponding to different steps of grid refinement is given, see Figure 6. Within the Figures 7 to 8 the grids as well as the numerical solutions resulting from two refinement steps are displayed. Since the gradients are not too strong, a good approximation of the real solution is reached by means of two adaption steps. In order to test the method in the context of thin boundary layers with steep gradients we choose the parameter $\theta = 20$ and we start from an equally coarse grid as before, see Figure 9 on page 23. Again, in Figure 10 the comparison of computed values along the x_1-axis for different levels of refinement is given, while the evolution of the refinement of the grid together with the corresponding numerical solutions can be seen in the Figures 11 to 13 (pages 24 and 25. The distribution along the x_1-axis depicted in Figure 10 as well as the coloured plots shown in the Figures 11, 12 and 13 prove that the dominant features are resolved in a reliable and accurate manner. Note that only one more level of refinement is needed to resolve a much thinner boundary layer.

4.2 Thermoregulation

Suddenly occuring lack of oxygen is known to be an important cause of injury to the developing brain of premature infants [13]. The neuronal loss suffered in such a critical situation evolves over several days [10]. One of the factors that influence the degree and distribution of neuronal loss is the cerebral temperature. Clinical studies have shown that lowering the cerebral temperature can prevent much damage [2]. In order to investigate if the temperature within the brain of a premature infant in an incubator can be lowered by manipulating the environmental parameters, Fischer et al. [8] employed a finite volume technique identical with the numerical method described within this paper but without an adaptive routine to solve a variation of the bio-heat equation which reads as

$$\partial_t T(\mathbf{x}, t) = \operatorname{div}(\lambda(\mathbf{x}) \nabla T(\mathbf{x}, t)) + q(\mathbf{x}, t) \tag{21}$$

and which features strong source terms given by

$$q(\mathbf{x}, t) = q_M(\mathbf{x}) + q_B(\mathbf{x}, t).$$

Thereby, $q_M(\mathbf{x})$ is the metabolical heat production and $q_B(\mathbf{x}, t)$ is a model of heat transfer within the human body due to blood flow. This model is based on the assumption of a steady state situation. Concerning the grid used within the work of Fischer et al. it should be noted that structured subgrids were used in the boundary region in order to capture steep heat gradients. For more details and for a theoretical discussion of the method see [8].

In the following, we discuss the simulation of heat transfer with respect to an infant of 1 kg by the use of the described adaptive scheme. It is evident to start from a coarse primary grid and to proceed by computing the corresponding steady state solution. If a steady state solution is reached, the grid is adapted by using the described AMA method and again a steady state calculation is started. We now investigate different levels of refinement computed and used by the method together with the corresponding numerical solutions. Within the Figures 14 and 15 (pages 26 and 27) the evolution the grid undergoes is displayed and it can be seen that a suitable solution

Mesh	Number of triangles
First Mesh	1822
Second Mesh	3673
Third Mesh	6731
Fourth Mesh	8956
Reference Mesh	37351

Table 1: Numbers of triangles used within the refinement steps compared to the grid employed by Fischer et al. [8]

is reached three refinement steps after starting from a quite coarse triangulation. In Table 4.2 the numbers of triangles used within the different steps of refinement is given together with the corresponding number of the mesh used by Fischer et al. which is denoted as the reference mesh.

5 Concluding remarks and Outlook

A finite volume method on unstructured grids for the simulation of heat conduction problems with steep gradients due to source terms is presented.
Several realistic applications show a distribution of the heat conductivity which is piecewise constant. In this context, the minimum maximum principle derived in [8] is improved in the sense that weaker assumption with respect to the underlying triangulation are required. Thus, a more general mesh adaptation method can be applied for the numerical solution of heat conduction problems.
The presented numerical examples show a high efficiency of the combination of the finite volume method with the anisotropic mesh adaptation technique. The numerical scheme (5) is sufficiently robust even for fast changing solution on grids satisfying only conditions A1 and A2 admitting also thin and long triangles which are often generated by AMA. On the other hand the application of AMA for numerical solution facilitates to achieve desired solution on a triangulation with not too high number of elements and therefore to save a memory and CPU-time of computers. This is a very important feature for 3D problems.
Numerical results from section 4.1 show, that there is not any fundamental problem to capture a solution with a very steep gradients. Moreover, we obtain sufficiently precise solution without large number of triangles. The

numerical solution of the thermoregulation of a premature infants from 4.2 was computed on a mesh with four times lower number of triangles than in Fischer et al. [8] whereas the results are very similar.
The outlook of the work is the extension to 3D problems which should simulate more realistic problems. There is no principle problem in 3D extension neither for finite volume scheme nor for anisotropic mesh adaptation technique. Preliminary work was already done in [20].

Acknowledgements

The research of V. Dolejší has been supported under the Grant No. 201/99/0267 and No. 201/00/D116 of the Czech Grant Agency and by the Grant MSM 113200007.
The work of M. Breuß and A. Meister was supported by the DFG-Graduiertenkolleg "Erhaltungsprnzipien in der Modellierung und Simulation mariner, atmosphärischer und technischer Systeme".
The authors gratefully acknowledge this supports.
Furthermore, M. Breuß and A. Meister would like to express their thanks to Prof. Dr. B. Fischer (Medical University Lübeck) and Dr. J. Koch (Dept. Basic Development, Drägerwerk AG, Lübeck) for their keen interest in the study.

References

[1] O. Bussmann. *A model for thermoregulation of premature and newborn infants under consideration of the thermal maturity.* Dissertation, Institute of Biomedical Engineering, Medical University of Lübeck, 2000. (in German)

[2] R. Busto, W. D. Dietrich, M. Y. Globus, M. D. Ginsberg. The importance of brain temperature in cerebral ischemic injury. *Stroke*, 20: 1134–1114, 1989.

[3] E. F. D'Azevedo, R. B. Simpson. On optimal triangular meshes for minimizing the gradient error. *Numer. Math.*, 59: 321–348, 1991.

[4] V. Dolejší. Anisotropic mesh adaptation for finite volume and finite element methods on triangular meshes. *Computing and Visualisation in Science*, 1: 165–178, 1998.

[5] V. Dolejší, J. Felcman. Anisotropic mesh adaptation and its application for scalar diffusion equations. *Numerical Methods for Partial Differential Equations (submitted)*, 2000.

[6] M. Feistauer, J. Felcman, V. Dolejší. Numerical simulation of compresssible viscous flow through cascades of profiles. *ZAMM*, 76: 297–300, 1996.

[7] M. Feistauer, J. Felcman, M. Lukáčová. Combined finite elements–finite volume solution of compressible flow. *J. Comput. Appl. Math.*, 63: 179–199, 1995.

[8] B. Fischer, M. Ludwig, A. Meister. An application of the finite volume method to the thermoregulation of infants. *Hamburger Beiträge zur Angewandten Mathematik, Reihe F, Computational Fluid Dynamics and Data Analysis 12, February* 2000.

[9] O. Friedrich, D. Hempel, A. Meister, Th. Sonar. Adaptive Computation of Unsteady Flow Fields with the DLR-$\mathcal{T}$-Code. *in: 77th AGARD Fluid Dynamics Panel Meeting and Symposium on Progress and Challenges in CFD Methods and Algorithms, AGARD-CP-578, Sevilla*, 1995.

[10] P. D. Gluckman, C. E. Williams. When and why do brain cells die? *Dev. Med. Child Neurol.*, 34: 1010–1014, 1992.

[11] D. D. Gray, A. Giorgini. The validity of the Boussinesq approximation for liquids and gases. *Int. J. Heat Mass Transfer*, 19: 545–551, 1976.

[12] D. Kröner. *Numerical Schemes for Conservation Laws.* Teubner, Stuttgart, 1997.

[13] E. C. Mallard, C. E. Williams, B. M. Johnston, P. D. Gluckman. Neuronal damage in the developing brain following intrauterine asphyxia. *Reprod. Fertil. Dev.*, 7: 647–653, 1995.

[14] A. Meister, M. Oevermann. An Implicit Finite Volume Approach of the $k - \epsilon$ Turbulence Model on Unstructured Grids. *Z. Angew. Math. Mech.*, 78 (11): 743–757, 1998.

[15] A. Meister, Th. Sonar. Finite-volume schemes for compressible fluid flow. *Surv. Math. Ind.*, 8: 1–36, 1998.

[16] Th. Sonar. *Mehrdimensionale ENO-Verfahren.* Teubner Verlag, Stuttgart, 1997.

[17] Th. Sonar. On the Construction of Essentially Non-Oscillatory Finite Volume Approximations to Hyperbolic Conservation Laws on General Trinagulations: Polynomial Recovery, Accuracy, and Stencil Selection. *Comp. Meth. Appl. Mech. Eng.*, 140: 157–181, 1997.

[18] J. Werner. Thermoregulatory models: recent research, current applications and future development. *Scand. J. Work. Environ. Health*, Vol.15: 34–46, 1989.

[19] J. Werner, P. Webb. A six-cylinder model of human thermoregulation for general use on personal computers. *Ann. Physiol. Anthrop.*, Vol.12 (3): 123–134, 1993.

[20] M. Zoubek. *Adaptive methods for the solution of threedimensional flow.* Master Thesis, Charles University, Prague, 2001. (in Czech)

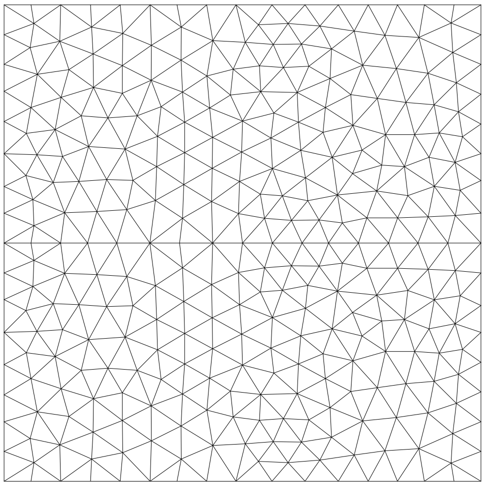

Figure 5: Initial triangulation

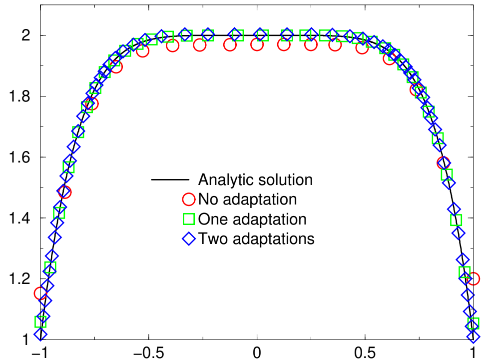

Figure 6: Temperature distribution along the x_1-axis related to the source term $y(x_1) = x_1^6$.

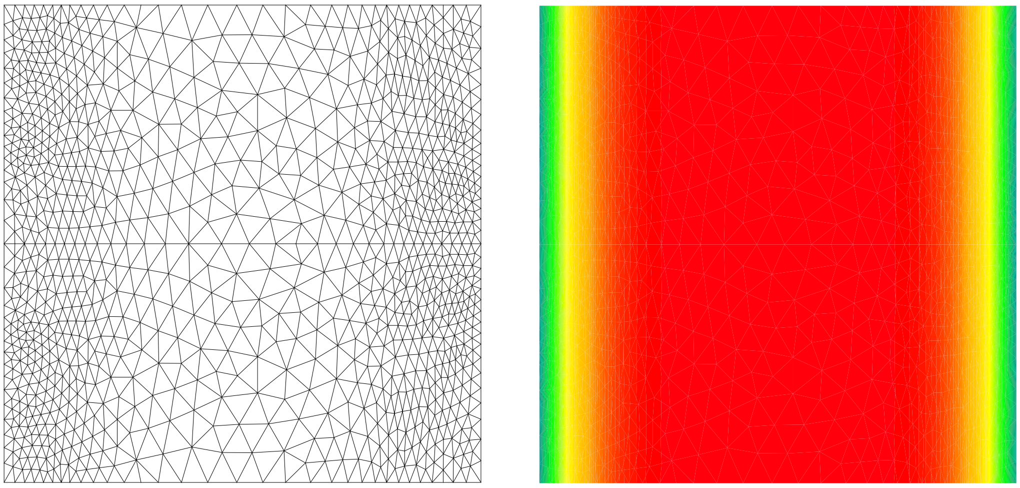

Figure 7: Grid after one adaptation and corresponding stationary temperature distribution

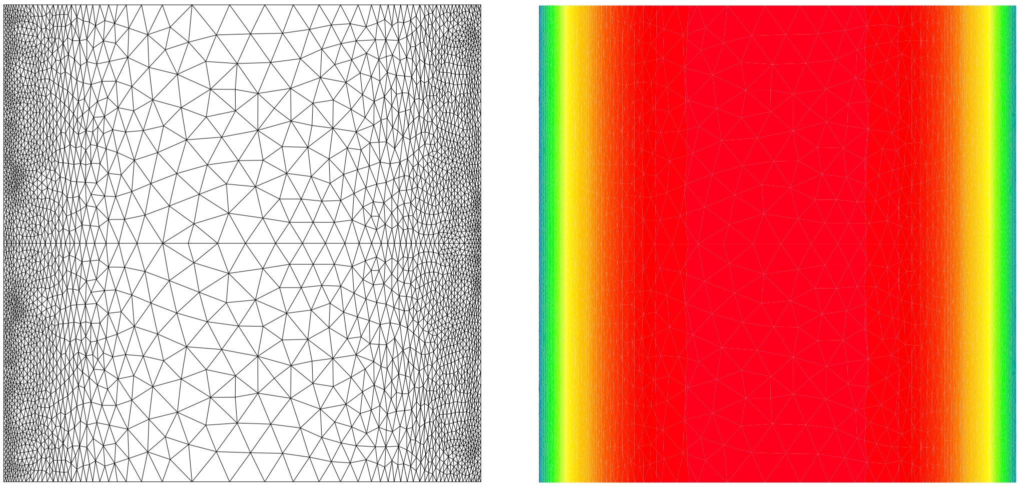

Figure 8: Grid after two adaptations and corresponding stationary temperature distribution

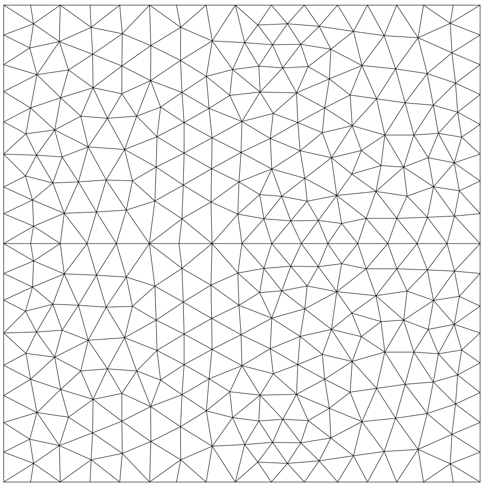

Figure 9: Initial triangulation

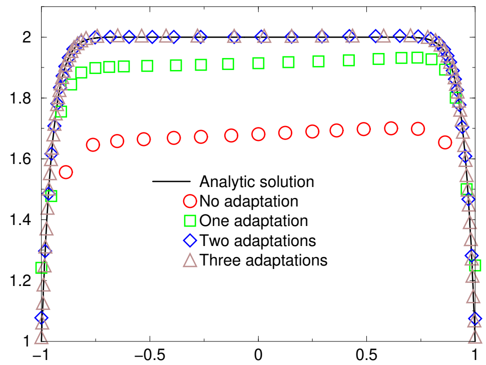

Figure 10: Temperature distribution along the x_1-axis related to the source term $y(x_1) = x_1^{20}$.

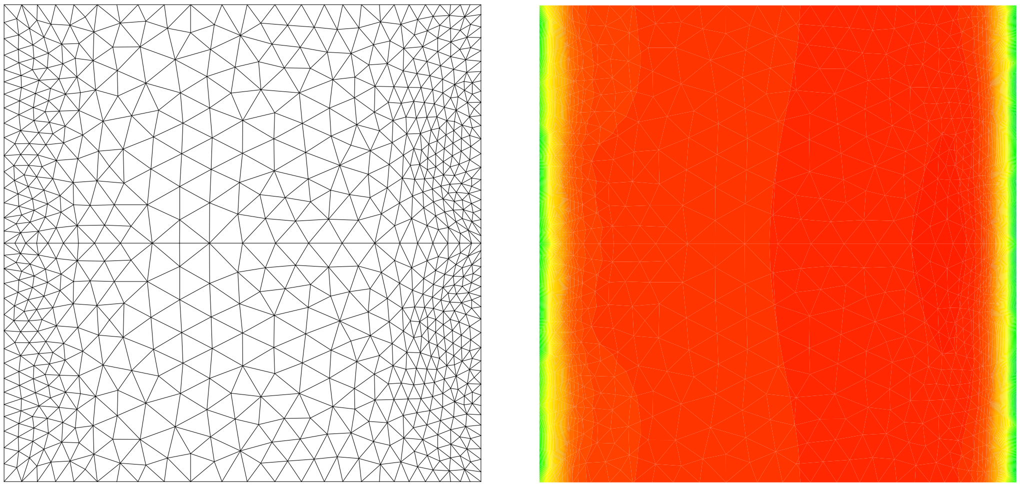

Figure 11: Grid after one adaptation and corresponding stationary temperature distribution

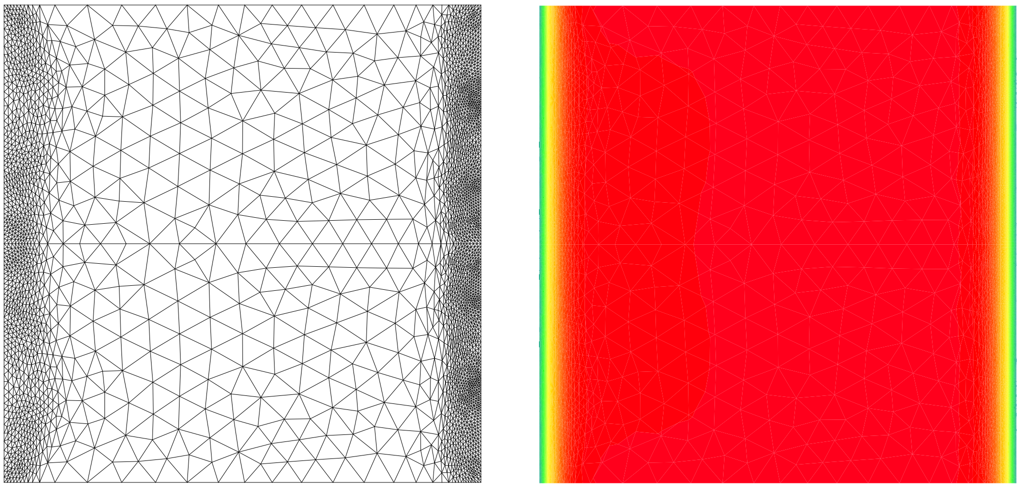

Figure 12: Grid after two adaptations and corresponding stationary temperature distribution

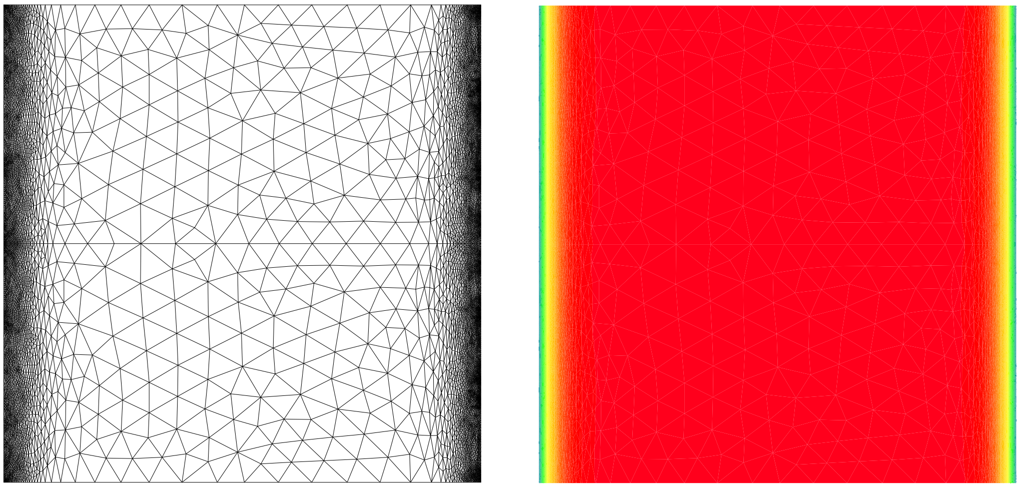

Figure 13: Grid after three adaptations and corresponding stationary temperature distribution

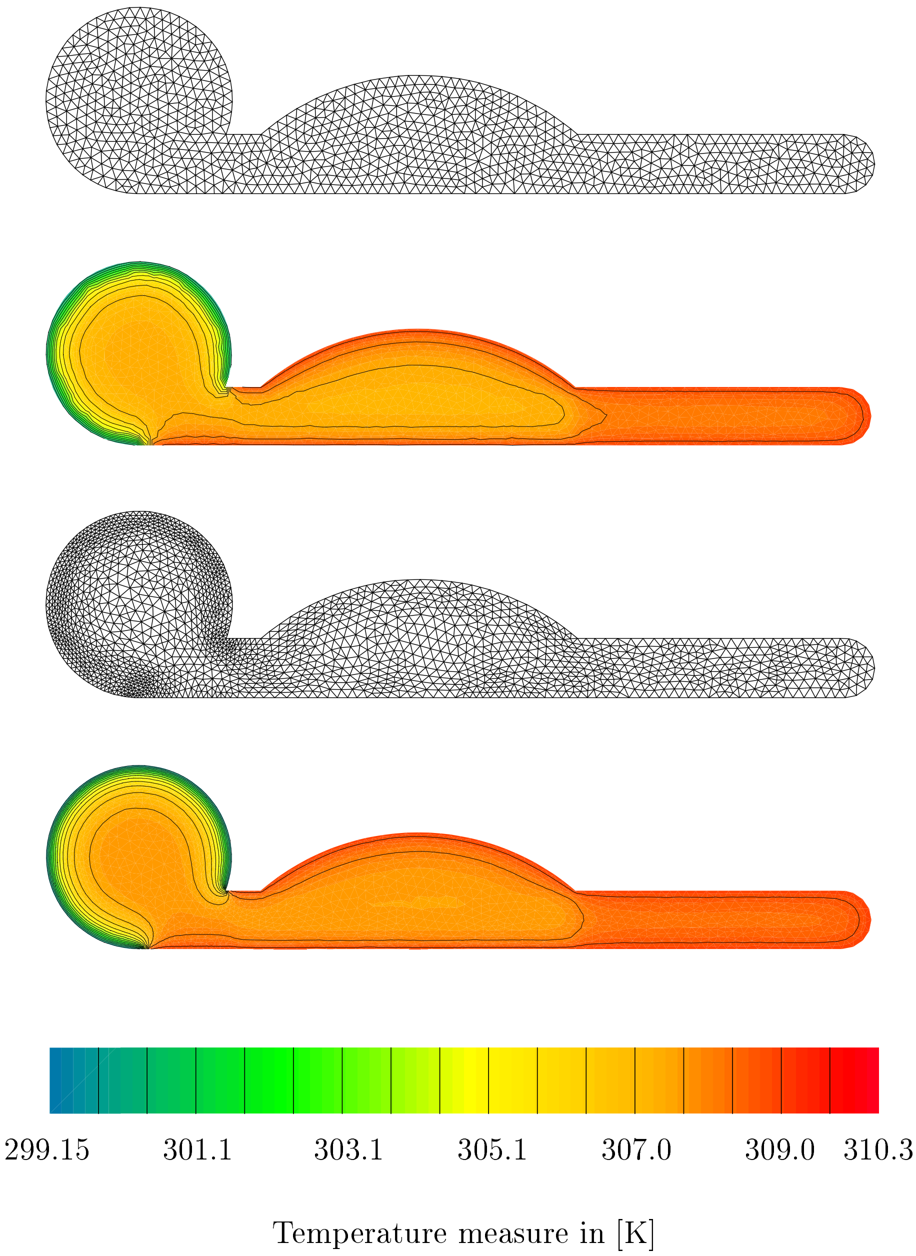

Figure 14: Sequence of triangulations and corresponding temperature distributions (part I)

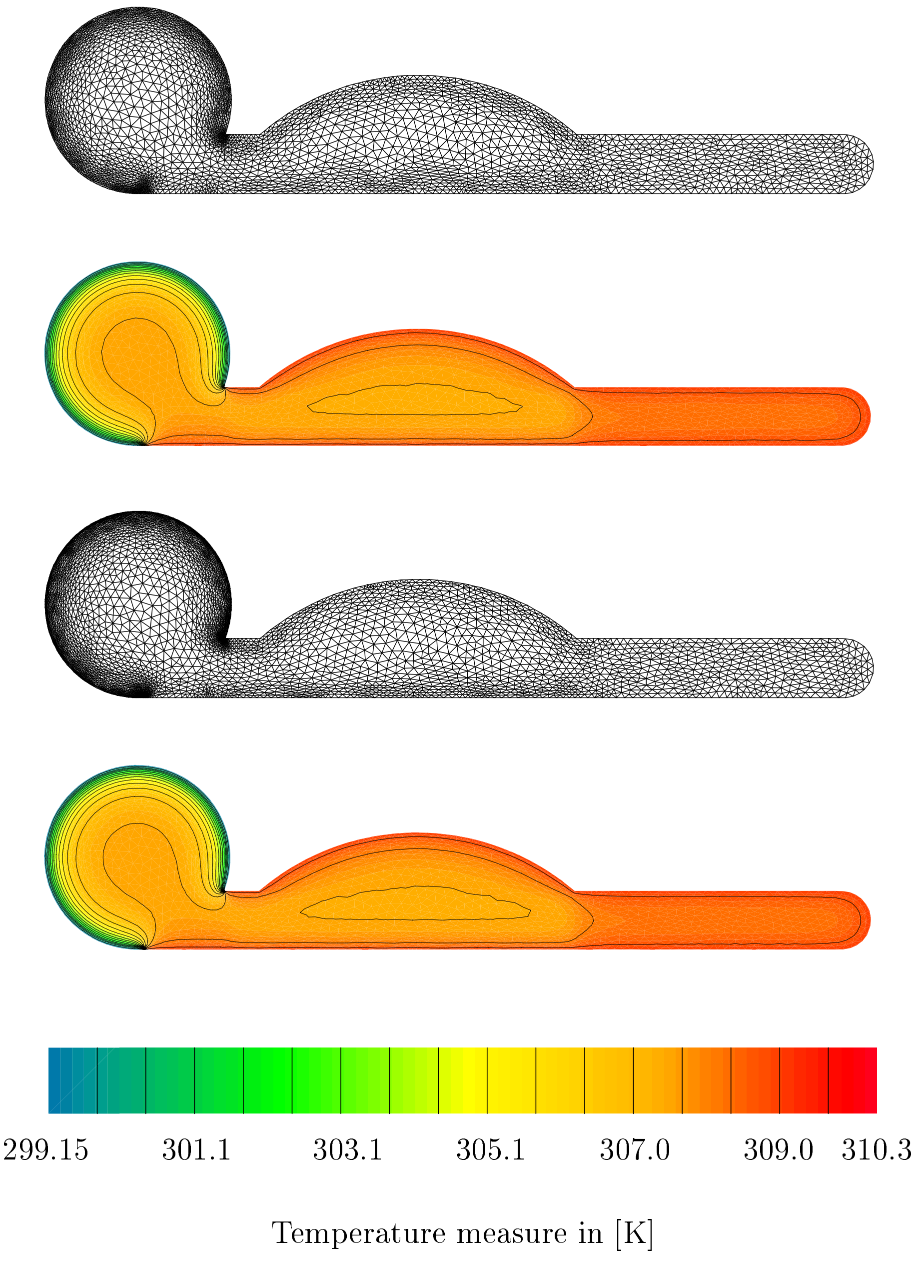

Figure 15: Sequence of triangulations and corresponding temperature distributions (part II)